Eur. Phys. J. Plus (2019) **134**: 50
DOI 10.1140/epjp/i2019-12473-9

THE EUROPEAN PHYSICAL JOURNAL PLUS

Regular Article

Convective heat transfer during the flow of Williamson nanofluid with thermal radiation and magnetic effects

Hashim[a], Masood Khan, and Aamir Hamid

Department of Mathematics, Quaid-i-Azam University, Islamabad 44000, Pakistan

Received: 10 August 2018 / Revised: 2 December 2018
Published online: 1 February 2019

Abstract. Recently, several studies have been presented to show that nanofluids are amongst the best tools for the enhancement of heat transfer characteristics. It has been experimentally verified that nanofluids are a new type of enhanced working fluids, engineered with enhanced thermo-physical properties. Therefore, we present a novel study to develop and understand a mathematical model for a non-Newtonian Williamson fluid flow in the presence of nanoparticles. This study aims at describing the thermal characteristics of nanoparticles via Rosseland approximation to illustrate the non-linear radiation effects. Convective heat transfer model alongside Brownian motion are studied for the electrically conducting nanofluids flow. A set of partial differential equations for Williamson nanofluid flow has been derived by basic conservation laws, *i.e.*, momentum, energy and concentration conservations. These equations are initially converted to ordinary differential equations by employing non-dimensional quantities. The numerical simulation of these equations is performed using the Runge-Kutta-Fehlberg scheme. The corresponding important physical parameters have been produced as function of the unsteadiness parameter, Weissenberg number, magnetic parameter, radiation parameter, Brownian motion parameter, thermophoresis parameter, Prandtl number, Biot number, velocity slip parameter and Lewis number. The examination is done to investigate the impact of the above-said parameters on momentum, thermal and concentration boundary layers. It is concluded from our computations that the nanofluids velocity and temperature accelerate when the Brownian motion parameter rises. Results proved that temperature gradient enhances with increase of solid particle concentration, while it decreases with increasing magnetic field. Finally, a comparison of the obtained numerical solution against previous literature is presented which shows satisfactory agreement.

1 Introduction

In recent years, a huge number of investigations has been dedicated to the theory of nanofluids due to their various technological and industrial applications. The various applications of nanofluids includes hybrid power engines, nuclear reactors, cooling of transformed oil, biomedicine and transportation, macro and microscale heat exchangers, radiators and electronic equipment and so forth. On the other hand, this innovation intends to enhance the thermal conductivities and the convective heat transfer of the working fluids, like water, toluene, ethylene, engine oil and glycerine. In this technique, nano-sized particles (1–100 nm) are dispersed into the working fluids and it is reported that their thermal conductivity is significantly higher than that of working fluids. According to several previous studies, it is found experimentally that the addition of a very small amount of nanoparticle into the ordinary fluids corresponds to significant enhancement in heat transfer. In 1995, Choi [1] first reported an innovative study which showed improvements in thermal conductivity of the base fluid in case of using ultra-fine nanoparticles in base fluid. In the recent past, many scientists and researchers make use of such nanoparticles to enhance the thermal properties in fluid flows. Keeping in view the study on nanofluids flows, a non-homogeneous equilibrium model for convective heat transport in nanofluids considering the Brownian motion and thermophoretic diffusion was developed by Buongiorno [2]. Later, Nield and Kuznetsove [3] presented the problem of the natural convection boundary layer flow over a vertical plate in the presence of nanoparticles. Makinde and Aziz [4] inspected the convective heat transfer characteristics of a nanofluids flow past a stretched surface. They have computed the numerical solutions of the governing problem. An investigation on electrically conducting nanofluid flow and heat transfer mechanisms past a stretching sheet has been

[a] e-mail: hashim@math.qau.edu.pk (corresponding author)

reported by Mahbood *et al.* [5]. In view of comprehensive applications of nanoparticles and improved thermal conductivity several researchers investigated the phenomena of nanofluids alongside various flow controlling parameters, like the thin film flow of a non-Newtonian nanofluid (Sandeep and Malvandi [6]), stretching surface with heat and mass transfer mechanism in Carreau nanofluid flow, Hashim and Khan [7], theoretical models for the thermal conductivity of carbon nanotubes (Nadeem *et al.* [8]) and the flow of William nanofluids past a wedge geometry (Hashim *et al.* [9]).

Researchers have determined that the problem of combined heat and mass transfer by considering thermal radiation phenomenon is an important topic due to its wide practical applications in chemical and engineering industries. Most engineering processes occurs because of temperature differences and hence the study of radiative heat transport plays a significant role in the structure and design of advanced energy systems. Mukhopadhy *et al.* [10] inspected the effect of nonlinear radiation on steady flow and heat transport behaviour across a permeable sheet. After a while, Cortell [11] presented a numerical investigation to study the radiative heat transfer features by utilizing the Rosseland approximation for electrically conducting viscous fluid flow. He concluded that the fluid temperature was significantly boosted by the rising thermal radiation. Besides, Hayat *et al.* [12] explored the three-dimensional flow of a viscous nanofluid by considering the effects of radiative heat transfer and momentum slip condition. Analytical solutions for momentum and thermal fields have been computed by employing the homotopy analysis methods. The oblique stagnation point flow of electrically conducting viscous nanofluid with convective heat transfer mode and thermal radiation have been probed by Khan *et al.* [13]. They computed a numerical solution to their governing problem by utilizing the Runge-Kutta-Fehlberg technique. In another study, Nayak *et al.* [14] reported a three-dimensional free convective flow model by considering the impacts of thermal radiation and transverse magnetic field. One striking part of this examination is that they employed a newly proposed micro-convection model, namely the Patel model, in the perspective of enhanced thermal conductivity. Currently, Dogonchi *et al.* [15] analysed theoretically the unsteady flow of viscous nanofluid between two parallel flat plates in view of thermal radiation. Lately, extensive researches have been done on thermal radiation effects during flow and heat transfer [16–18].

Due to the diversity in characteristics of the non-Newtonian liquids, various models have been developed to study their physical properties. Out of these, the Williamson [19] fluid model has gained considerable attention because it can efficiently exhibit the shear thinning property. In view of this, different studies have been reported by Dapra and Scarpi [20], Vasudev *et al.* [21], Nadeem and Akbar [22], Nadeem and Hussain [23] to obtain the analytical solution of Williamson nanofluid flow by using homotopic analysis method (OHAM). After that, Bhatti and Rashidi [24] discussed the combined effects of thermo-diffusion and thermal radiation on Williamson nanofluid flow. They simulated the results of their problem by utilizing spectral methods. The two-dimensional flow of a Williamson nanofluid generated by a stretched surface alongside variable thermal conductivity was examined by Reddy *et al.* [25]. Furthermore, Kumar and Sundeep [26] theoretically explored the features of heat and mass transfer for MHD flow of Williamson and Casson fluids along a paraboloid surface.

On assessing the literature exhibited above, the foremost concern of this analysis is to deliberate the time-dependent convective axisymmetric flow in a Williamson nanofluid over a radially stretching wall. The surface nanoparticles concentration is assumed to be uniform and the convective boundary condition is considered. Moreover, this article aims at adding a new dimension to the boundary layer flow of the Williamson fluid by considering the radiative heat transfer in the form of the Rosseland approximation [27]. To the best of the authors' knowledge, no attempt has been reported before to investigate such flow situations for the non-Newtonian Williamson model. The numerical simulation is done by the computer software MATLAB by utilizing the Cash-Karp technique. The control of active parameters on momentum, thermal and concentration fields are deliberated in detail with the aid of plotted graphs and tables. Further, a comparison with the existing literature in limiting sense is found in an excellent agreement.

2 Mathematical model

2.1 Williamson constitutive equation

In this study, we consider the flow behaviour of a non-Newtonian Williamson model. This rheological model has significant theoretical basis and describes the conduct of various non-Newtonian fluids. The Williamson fluid behaviour is represented by non-Newtonian viscosity μ, namely apparent viscosity

$$\mu = \mu_\infty + \frac{\mu_0 - \mu_\infty}{1 + \Gamma|\dot{\gamma}|}, \tag{1}$$

where $\Gamma > 0$ is a time constant and μ_0 and μ_∞ are the viscosities at zero and infinite shear rates, respectively. The shear rate $\dot{\gamma}$ is defined as follows:

$$\dot{\gamma} = \sqrt{\frac{1}{2}\mathbf{D} : \mathbf{D}}, \quad \text{where } \mathbf{D} = \nabla\mathbf{V} + (\nabla\mathbf{V})^{\mathrm{T}}. \tag{2}$$

By considering the infinite shear rate viscosity and $\Gamma\dot{\gamma} < 1$, eq. (1) takes the form

$$\mu = \mu_0 \left[\beta^* + \frac{1-\beta^*}{1-\Gamma\dot{\gamma}}\right], \tag{3}$$

where $\beta^* = \frac{\mu_\infty}{\mu_0}$ denotes the ratio of viscosities.

2.2 Basic flow equations

The continuity and momentum equation for the time-dependent flow of a Williamson fluid can be expressed in dimensional forms as follows:

$$\boldsymbol{\nabla}\cdot\mathbf{V} = 0, \tag{4}$$

$$\rho\frac{\mathrm{d}\mathbf{V}}{\mathrm{d}t} = -\nabla p + \boldsymbol{\nabla}\cdot\boldsymbol{\tau} + \mathbf{J}\times\mathbf{B}, \tag{5}$$

where $\mathbf{V}$ is the flow velocity vector, ρ the density, p the pressure, $\boldsymbol{\nabla}$ the gradient operator, $\boldsymbol{\tau}$ the stress tensor, $\mathbf{J}$ the current density and $\mathbf{B}$ the total magnetic field.

The shear stress tensor $\boldsymbol{\tau}$ is

$$\boldsymbol{\tau} = \mu\left(\dot{\gamma}\right)\mathbf{D}. \tag{6}$$

The flow velocity vector is of the form

$$\mathbf{V} = \left[u(r,z,t), 0, w(r,z,t)\right], \tag{7}$$

where u and w means the radial and axial components of flow velocity, respectively.

The shear rate or rate of deformation tensor in (r,z) coordinates is given by

$$\dot{\gamma} = \left[2\left(\frac{\partial u}{\partial r}\right)^2 + 2\left(\frac{\partial w}{\partial z}\right)^2 + \left(\frac{\partial u}{\partial z} + \frac{\partial w}{\partial r}\right)^2 + \frac{2u^2}{r^2}\right]^{1/2}. \tag{8}$$

Combining eqs. (6) and (7) and employing the Boussinesq approximations, the governing continuity and momentum equations become:

$$\frac{\partial u}{\partial r} + \frac{u}{r} + \frac{\partial w}{\partial z} = 0, \tag{9}$$

$$\frac{\partial u}{\partial t} + u\frac{\partial u}{\partial r} + w\frac{\partial u}{\partial z} = \nu\frac{\partial^2 u}{\partial z^2}\left[\beta^* + (1-\beta^*)\left(1-\Gamma\frac{\partial u}{\partial z}\right)^{-1}\right] + \nu\Gamma\left(\frac{\partial u}{\partial z}\right)\frac{\partial^2 u}{\partial z^2}\left[(1-\beta^*)\left(1-\Gamma\frac{\partial u}{\partial z}\right)^{-2}\right] - \frac{\sigma B^2(t)}{\rho}u, \tag{10}$$

$$0 = -\frac{1}{\rho}\frac{\partial p}{\partial z}, \tag{11}$$

where the kinematic viscosity is denoted by $\nu = \frac{\mu_0}{\rho}$ and $B(t)$ denotes the time-dependent magnetic field.

2.3 Flow and thermal transport of nanofluids

We consider the unsteady axisymmetric flow of an incompressible and electrically conducting Williamson nanofluid induced by a convectively heated radially stretching sheet. Impacts of non-linear thermal radiation and slip boundary condition are also considered. The flow analysis has been performed in a two-dimensional (r,z) frame of reference, as shown in fig. 1. The radially stretching sheet is placed at $z = 0$ and the fluid flows in the upper half-region $z > 0$. Further, the flow field is exposed to the influence of an external magnetic field of strength $B(t) = \frac{B_0}{(1-\beta t)^{1/2}}$ applied perpendicular to the plane of the sheet (*i.e.*, along the z-axis). In writing the momentum equation, we have neglected the induced magnetic field for small Reynolds number. Also, heat transfer analysis of nanoparticles is studied by incorporating Brownian motion and thermophoresis effects. Additionally, the velocity slip condition at the surface is also implemented. The stretching velocity of the sheet in radial direction is given by $u_w(r,t) = \frac{ar}{1-ct}$, where a and c are constants having the dimensions of (time^{-1}).

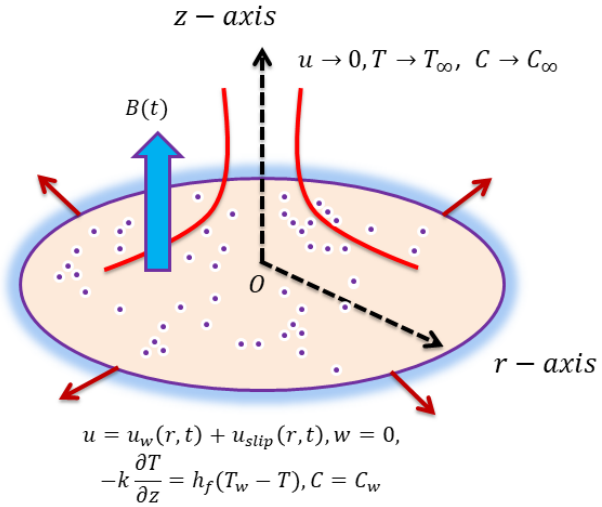

Fig. 1. A physical layout of the flow configuration.

Taking the above assumptions into consideration, the dimensional governing equations for the nanofluid flow and convective heat transfer are given by

$$\frac{\partial u}{\partial r}+\frac{u}{r}+\frac{\partial w}{\partial z}=0, \tag{12}$$

$$\frac{\partial u}{\partial t}+u\frac{\partial u}{\partial r}+w\frac{\partial u}{\partial z}=\nu\frac{\partial^2 u}{\partial z^2}\left[\beta^*+(1-\beta^*)\left(1-\Gamma\frac{\partial u}{\partial z}\right)^{-1}\right] + \nu\Gamma\left(\frac{\partial u}{\partial z}\right)\frac{\partial^2 u}{\partial z^2}\left[(1-\beta^*)\left(1-\Gamma\frac{\partial u}{\partial z}\right)^{-2}\right]-\frac{\sigma B^2(t)}{\rho}u, \tag{13}$$

$$\frac{\partial T}{\partial t}+u\frac{\partial T}{\partial r}+w\frac{\partial T}{\partial z}=\frac{\partial}{\partial z}\left[\left(\alpha_m+\frac{16\sigma^* T^3}{3k^*\rho c_p}\right)\frac{\partial T}{\partial z}\right]+\tau\left[D_B\frac{\partial C}{\partial z}\frac{\partial T}{\partial z}+\frac{D_T}{T_\infty}\left(\frac{\partial T}{\partial z}\right)^2\right], \tag{14}$$

$$\frac{\partial C}{\partial t}+u\frac{\partial C}{\partial r}+v\frac{\partial C}{\partial z}=D_B\frac{\partial^2 C}{\partial z^2}+\frac{D_T}{T_\infty}\frac{\partial^2 T}{\partial z^2}. \tag{15}$$

In the above equations, $\tau=(\rho c)_p/(\rho c)_f$ is the ratio of heat capacitances of nanoparticle to base fluid, $\alpha_m=k/(\rho c)_p$ the thermal diffusivity, σ^* the Stefan-Boltzman constant, k^* the mean absorption coefficient, D_T the thermophoresis diffusion coefficient, D_B the Brownian diffusion coefficient and t the time.

We assume the physical boundary conditions for our problem as

$$u=u_w(r,t)+u_{\text{slip}},\quad w=0,\quad k\frac{\partial T}{\partial z}=-h_f(T_w-T),\quad C=C_w,\quad \text{at } z=0, \tag{16}$$

$$u\to 0,\quad T\to T_\infty,\quad C\to C_\infty,\quad \text{as } z\to\infty, \tag{17}$$

where T_∞ and C_∞ depict the fluid temperature and concentration at infinity, respectively. The velocity partial slip condition is of the form

$$u_{\text{slip}}=L\tau_{rz}=L\frac{\partial u}{\partial z}\left[\beta^*+(1-\beta^*)\left(1-\Gamma\frac{\partial u}{\partial z}\right)^{-1}\right], \tag{18}$$

where L is known as slip length.

The following non-dimensional variables are used:

$$\eta=\frac{z}{r}\,\text{Re}^{1/2},\qquad \psi(r,z,t)=-r^2u_w\,\text{Re}^{-1/2}\,f(\eta),\quad \theta(\eta)=\frac{T-T_\infty}{T_w-T_\infty}\quad\text{and}\quad \varphi(\eta)=\frac{C-C_\infty}{C_w-C_\infty}, \tag{19}$$

where the stream function ψ is defined as $u=\frac{-1}{r}\frac{\partial\psi}{\partial z}$ and $w=\frac{1}{r}\frac{\partial\psi}{\partial r}$.

Also, $T=T_\infty+[1+(\theta_w-1)\theta]$ with $\theta_w=\frac{T_w}{T_\infty}(>1)$ as the temperature ratio parameter.

Using the dimensionless variables, we get the following system of governing equations:

$$\left[\beta^* + (1-\beta^*)\left(1 - We f''\right)^{-2}\right] f''' - A\left(f' + \frac{\eta}{2} f''\right) + 2ff'' - (f')^2 - M^2 f' = 0, \tag{20}$$

$$\theta'' + \mathrm{Pr}\left(2f\theta' - \frac{A}{2}\eta\theta' + Nb\theta'\varphi' + Nt\,(\theta')^2\right) + \frac{4}{3N_R}\frac{\mathrm{d}}{\mathrm{d}\eta}\left[\{1 + (\theta_w - 1)\theta\}^3\theta'\right] = 0, \tag{21}$$

$$\varphi'' + 2Scf\varphi' - \frac{A}{2}Sc\eta\varphi' + \frac{Nt}{Nb}\theta'' = 0. \tag{22}$$

Consequently, the boundary conditions take the form

$$f(0) = 0, \quad f'(0) = 1 + s_1 f''(0)\left[\beta^* + (1-\beta^*)\left\{1 - We f''(0)\right\}^{-1}\right], \quad \theta'(0) = -\gamma(1 - \theta(0)), \tag{23}$$

$$\varphi(0) = 1, \quad f'(\infty) \to 0, \quad \theta(\infty) \to 0, \quad \varphi(\infty) \to 0. \tag{24}$$

The involved dimensionless parameters are given by

The local Weissenberg number $We^2 = \frac{a^3\Gamma^2 r^2}{\nu(1-ct)^3}$, the unsteadiness parameter $A = \frac{c}{a}$, the magnetic parameter $M = \sqrt{\frac{\sigma B_0^2}{\rho a}}$, the Prandtl number $\mathrm{Pr} = \frac{\nu}{\alpha_m}$, the non-linear radiation parameter $N_R = \frac{kk^*}{4\sigma^* T_\infty^3}$, the Schmidt number $Sc = \frac{\nu}{D_B}$, the thermophoresis parameter $Nt = \frac{\tau D_B(T_w - T_\infty)}{\nu T_\infty}$, the Brownian motion parameter $Nb = \frac{\tau D_B(C_w - C_\infty)}{\nu}$, the generalized Biot number $\gamma = \frac{rh_f}{k}\,\mathrm{Re}^{-1/2}$ and the velocity slip parameter $s_1 = \frac{L}{r}\,\mathrm{Re}^{1/2}$.

The physical parameters of engineering concern in this analysis are the skin friction (C_{fr}), Nusselt number (Nu_r) and Sherwood number (Sh_r), which are expressed as

$$C_{fr} = \frac{\tau_w|_{z=0}}{\rho u_w^2}, \qquad Nu_r = \frac{rq_w|_{z=0}}{k(T_w - T_\infty)}, \qquad Sh_r = \frac{rq_m|_{z=0}}{D_B(C_w - C_\infty)}, \tag{25}$$

where τ_w, q_w and q_m are the wall shear stress, wall heat flux and wall mass flux, respectively, having the following form:

$$\begin{aligned}
\tau_w &= \mu_0 \frac{\partial u}{\partial z}\left[\beta^* + (1-\beta^*)\left(1 - \Gamma\frac{\partial u}{\partial z}\right)^{-1}\right], \\
q_w &= -k\left(\frac{\partial T}{\partial z}\right) + (q_r), \quad \text{or} \quad q_w = -k\left(1 + \frac{16\sigma^*}{3k^*}T^3\right)\frac{\partial T}{\partial z}, \\
q_m &= -D_B\left(\frac{\partial C}{\partial z}\right).
\end{aligned} \tag{26}$$

On substituting eq. (19) into eqs. (25) and (26), we get

$$\begin{aligned}
\mathrm{Re}^{1/2}\, C_{fr} &= f''(0)\left[\beta^* + (1-\beta^*)\left\{1 - We f''(0)\right\}^{-1}\right], \\
\mathrm{Re}^{-1/2}\, Nu_r &= -\theta'(0)\left[1 + (4/3N_R)\left\{1 + (\theta_w - 1)\theta(0)\right\}^3\right], \\
\mathrm{Re}^{-1/2}\, Sh_r &= -\varphi'(0),
\end{aligned} \tag{27}$$

where $\mathrm{Re} = \frac{ru_w}{\nu}$ is the local Reynolds number.

3 Numerical simulation

We obtain a numerical solution to eqs. (20)–(22) and the corresponding boundary conditions (23) and (24) using the Runge-Kutta-Fehlberg integration method by employing Cash-Karp coefficients. Generally, the problems involving nonlinear ordinary differential equations are difficult to solve. Numerical solution of these equations is calculated by switching them into a system of first-order ordinary differential equations. Let us transfer the governing problem by introducing new variables:

$$f = X_1, \qquad f' = X_2, \qquad f'' = X_3, \qquad \theta = X_4, \qquad \theta' = X_5, \qquad \varphi = X_6, \qquad \varphi' = X_7. \tag{28}$$

Table 1. A comparison of the skin friction $\mathrm{Re}^{1/2}\,C_{fr}$ for different values of velocity slip parameter s_1 when $We = M = A = \beta^* = 0$.

	$-f''(0)$				
s_1	Exact [28]	HPM [28]	Perturbation [28]	Asymptotic [28]	Present results
0.0	1.173721	1.178511	1.173721	–	1.17373
0.01	1.153472	1.157311	1.153481	–	1.15348
0.02	1.134017	1.136998	1.134090	–	1.13403
0.05	1.079949	1.080820	1.081010	–	1.07996
0.1	1.001834	1.000308	1.009522	–	1.00185
0.2	0.878425	0.874453	0.930213	–	0.87844
0.5	0.650528	0.645304	1.201623	1.529918	0.65055
1.0	0.462510	0.458333	–	0.574163	0.46254
2.0	0.299050	0.296534	–	0.310753	0.2909
5.0	0.149393	0.148454	–	0.149590	0.14945
10.0	0.082912	0.082532	–	0.082833	0.08297
20.0	0.044368	0.044228	–	0.044337	0.04442
50.0	0.018732	0.018698	–	0.018727	0.01877
100.0	0.009594	0.009583	–	0.009593	0.009619

Therefore, the corresponding system of simultaneous first order ODEs are

$$X_1' = X_2, \qquad X_2' = X_3, \qquad X_3' = \frac{X_2^2 + A(X_2 + \frac{\eta}{2}X_3) + M^2 X_2 - 2X_1 X_3}{[\beta^* + (1-\beta^*)(1 - WeX_3)^{-2}]}, \tag{29}$$

$$X_4' = X_5, \qquad X_5' = \frac{-3N_R\,\mathrm{Pr}[2X_1X_5 - \frac{A}{2}\eta X_5 + NbX_5X_7 + NtX_5^2] - 12(\theta_w - 1)[1 + (\theta_w - 1)X_4]^2 X_5^2}{3N_R + 4[1 + (\theta_w - 1)X_4]^3}, \tag{30}$$

$$X_6' = X_7, \qquad X_7' = -2ScX_1X_7 - \frac{A}{2}Sc\eta X_7 - \frac{Nt}{Nb}X_5', \tag{31}$$

with the boundary conditions

$$X_1(0) = 0, \qquad X_2(0) = 1 + s_1 X_3(0)\left[\beta^* + (1-\beta^*)\{1 - WeX_3(0)\}^{-1}\right],$$
$$X_5(0) = -\gamma(1 - X_4(0)), \qquad X_6(0) = 1, \tag{32}$$
$$X_2(\infty) = 0, \qquad X_4(\infty) = 0, \qquad X_6(\infty) = 0. \tag{33}$$

The shooting scheme is employed to guess missing initial conditions by an iterative process until the boundary conditions are satisfied. Thus, we need a value for $X_3(0)$, *i.e.*, $f''(0)$, $X_5(0)$, *i.e.*, $\theta'(0)$ and $X_7(0)$, *i.e.*, $\varphi'(0)$. But no such values of $f''(0)$, $\theta'(0)$ and $\varphi'(0)$ are mentioned in the boundary conditions. Thus, we make a few conjectures for $f''(0)$, $\theta'(0)$ and $\varphi'(0)$. Thereafter, integration is completed, and it is seen that these guesses match the boundary conditions at the very end. The solutions are obtained by taking different initial guesses for the values of $f''(0)$, $\theta'(0)$ and $\varphi'(0)$, where the far field boundary conditions (33) must be satisfied by all profiles asymptotically. The step size is taken as 0.01 and the accuracy of sixth decimal place as the criterion of the convergence.

3.1 Validation of numerical scheme

To validate the present numerical procedure, the above simulation results have been tested with the results reported by Arial [28], who discuss the axisymmetric flow of a Newtonian fluid caused by a stretching surface with partial slip effects. The skin friction coefficient has been compared with the numerical data of Arial [28] for varying values of slip parameter s_1 by taking $We = A = M = \beta^* = 0$. Table 1 shows that the correspondence between the two sets of results is seen to be excellent.

In addition, the computed numerical results have been compared with those of Makinde *et al.* [29], who studied the flow of electrically conducting nanofluids driven by a radially stretching convective surface with thermal radiation. In table 2, the skin friction values of the case when $We = A = s_1 = \beta^* = 0$ are listed for different magnetic parameter M. As shown in this table, the results of current investigation are consistent with the data of Makinde *et al.* Therefore, the numerical scheme of the current analysis can be confirmed.

Table 2. A comparison of the skin friction $\mathrm{Re}^{1/2}\, C_{fr}$ for different values of M^2 when $We = A = s_1 = \beta^* = 0$.

M^2	$\mathrm{Re}^{1/2}\, C_{fr}$	
	Makinde *et al.* [29]	Present results
0.0	−1.17372	−1.17372
0.5	−1.36581	−1.36581
1.0	−1.53571	−1.53571
2.0	−1.83049	−1.83049
3.0	−2.08484	−2.08485

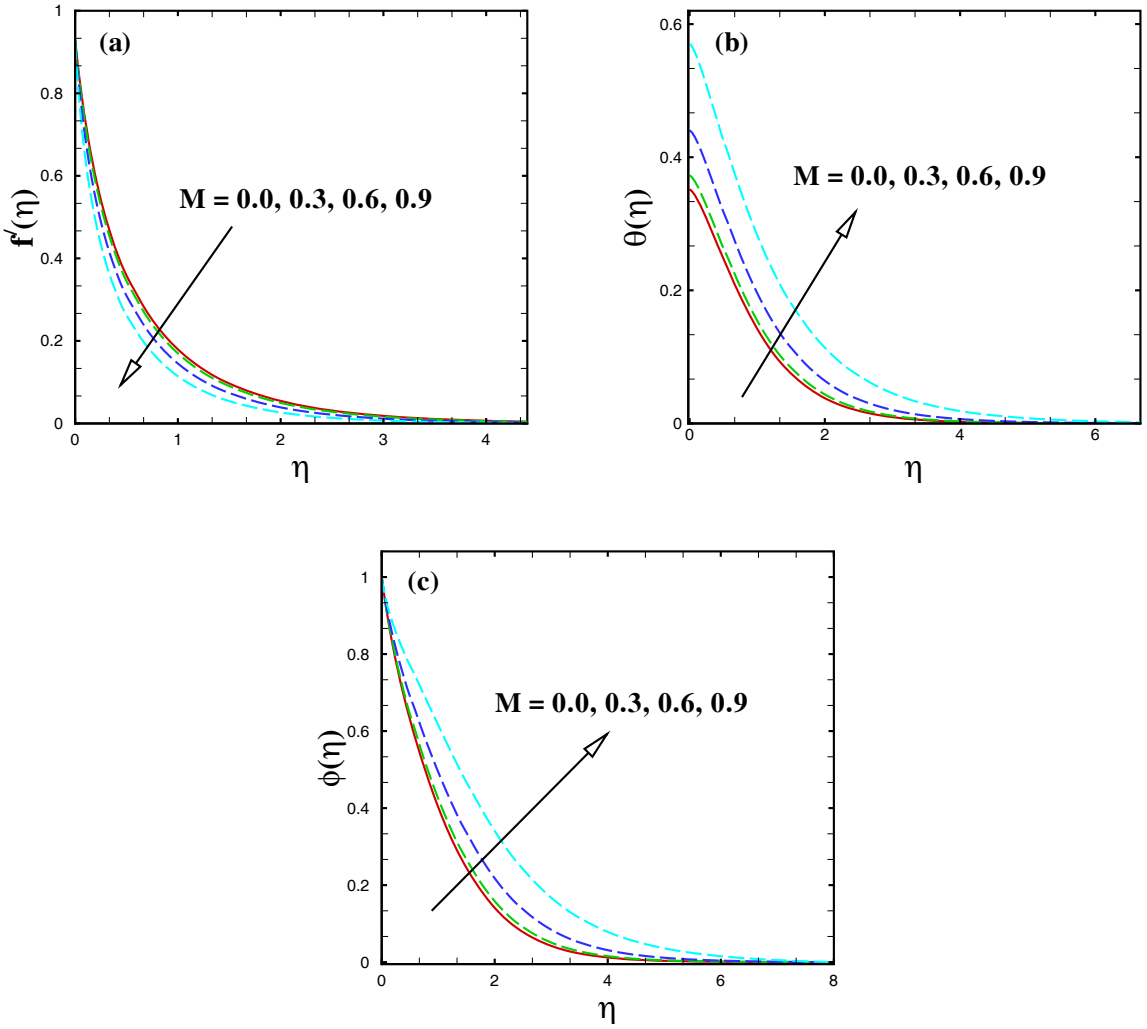

Fig. 2. The variation of M on velocity, temperature and concentration profiles.

4 Result analysis and discussion

This study is devoted to discussing the physical features of Williamson fluid flow caused by a radial stretched surface in the presence of non-linear thermal radiation and nanoparticles. In this section, the impacts of several leading non-dimensional parameters, namely, unsteadiness parameter A, viscosity ratio parameter β^*, magnetic parameter M, Weissenberg number We, Prandtl number Pr, velocity slip parameter s_1, temperature ratio parameter θ_w, thermal radiation parameter N_R on velocity, temperature and nanoparticles concentration are depicted graphically. The profiles for dimensionless velocity $f'(\eta)$, dimensionless temperature $\theta(\eta)$ and dimensionless concentration $\varphi(\eta)$ are presented in figs. 2–9 for fixed values of the physical parameters $We = 1.0$, $A = 0.1$, $\beta^* = 0.001$, $s_1 = 0.1$, $M = 0.2$, $\gamma = 0.1$, $\mathrm{Pr} = 2.5$, $Nt = 0.2$, $Nb = 0.1$, $N_R = 2.0$, $\theta_w = 1.2$ and $Sc = 2.0$.

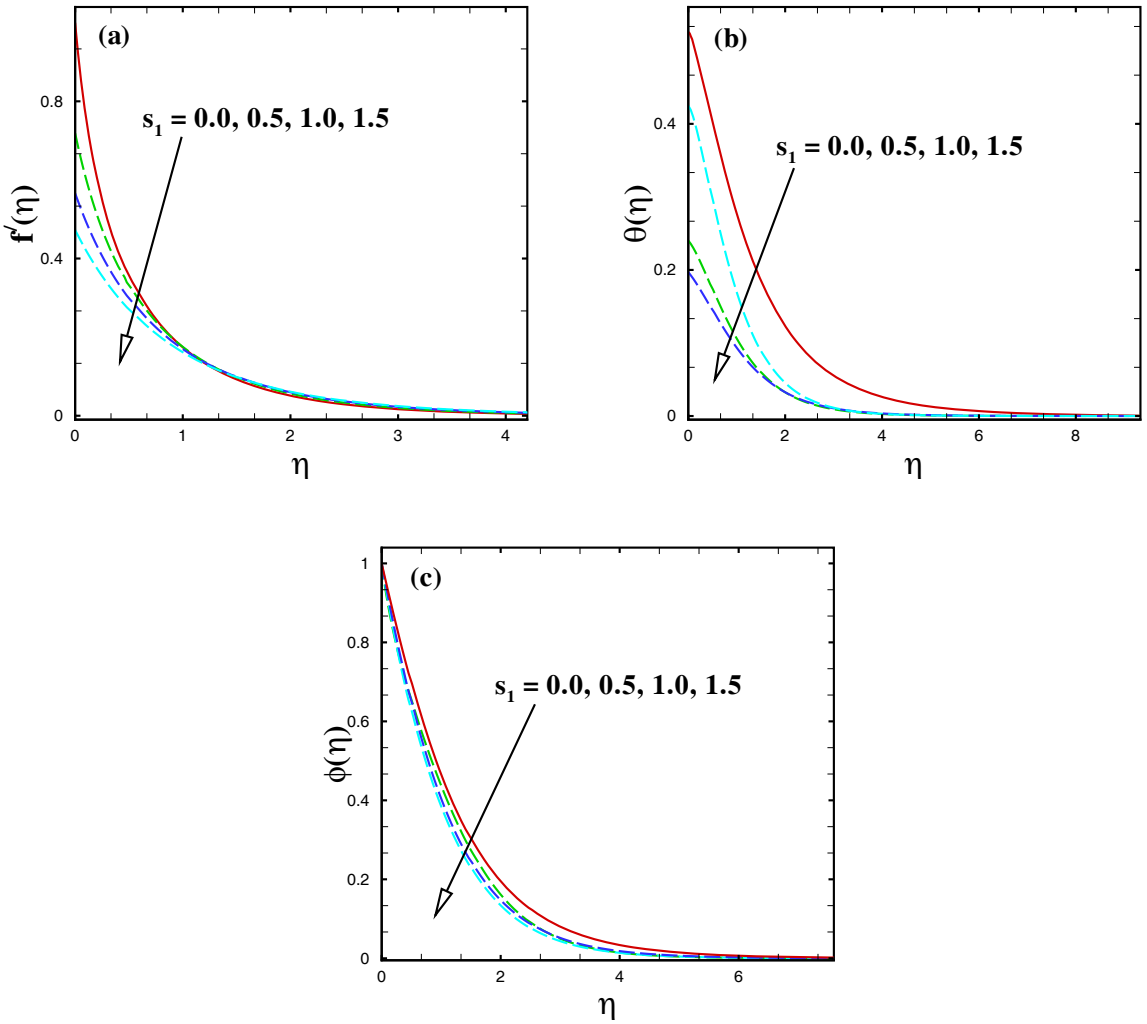

Fig. 3. The variation of s_1 on velocity, temperature and concentration profiles.

Figures 2(a)–(c) show the velocity, temperature and concentration distributions by varying the numerical values of magnetic field parameter M. Figure 2(a) shows that the velocity of nanofluids decreases with increasing the value of the magnetic parameter by keeping the other parameters fixed. Likewise, the associated momentum boundary layer thickness reduces with higher M. Physically, it is justified that the higher magnetic parameter has the capacity to slow down the motion of fluid particles: this happens due to the Lorentz force, which acts like a retarding force. From figs. 2(b) and (c), we observe that both temperature $\theta(\eta)$ and concentration $\varphi(\eta)$ are boosted with raising values of the magnetic parameter within the boundary layer region. In addition, a similar trend is noted for both thermal and solutal boundary layer thickness with higher M.

Figures 3(a)–(c) show the variation of velocity $f'(\eta)$, temperature $\theta(\eta)$ and nanoparticle concentration $\varphi(\eta)$ with different values of velocity slip parameter s_1. From this figure, it is obvious that the velocity of the fluid increases by increasing the values of the velocity slip parameter. Additionally, it can also be reported that temperature and nanoparticle concentration and their corresponding thermal and concentration boundary layer thicknesses are reducing functions of velocity slip parameter.

Figures 4(a) and (b) show the variation of temperature $\theta(\eta)$ and nanoparticle concentration $\varphi(\eta)$ with varying the values of the unsteadiness parameter A. It is clear, from these figures, that the fluid temperature and nanoparticles concentration show a rising behaviour with higher unsteadiness parameter. However, the corresponding boundary layer thickness increases by increasing the unsteadiness parameter. In fact, an increment in unsteadiness can boost the thermal as well as concentration boundary layer thicknesses.

Figures 5(a) and (b) are drawn to present the effects of temperature ratio parameter θ_w and radiation parameter N_R on the temperature profiles. From these figures, it is observed that increasing the values of the temperature ratio parameter leads to higher wall temperature as compared to the ambient fluid. As a result, the temperature of the fluid increases. It is also observed that the thermal boundary layer thickness accelerating for the stronger values of

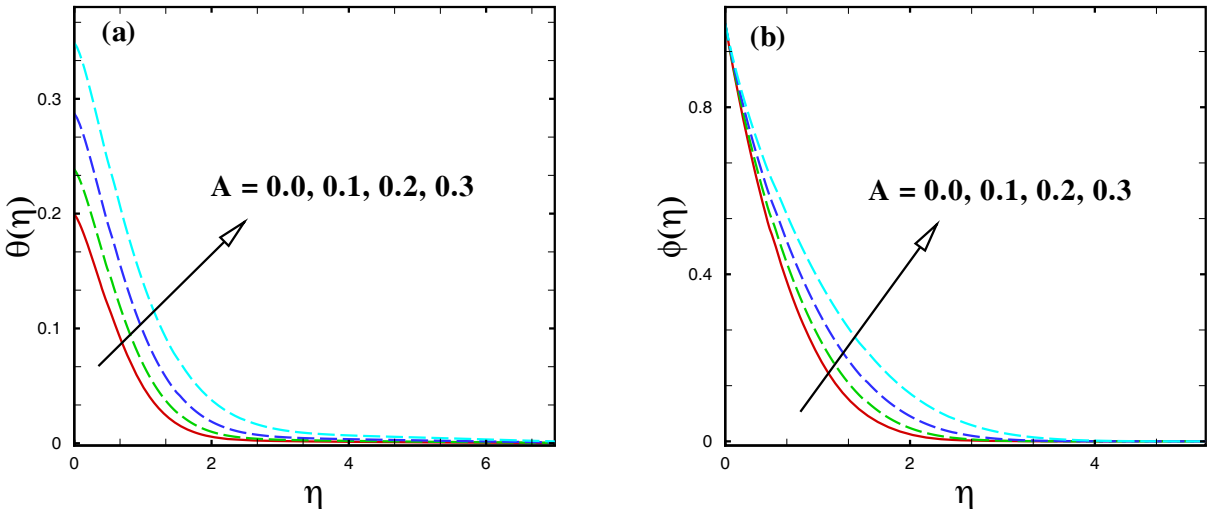

Fig. 4. The variation of A on temperature and concentration profiles.

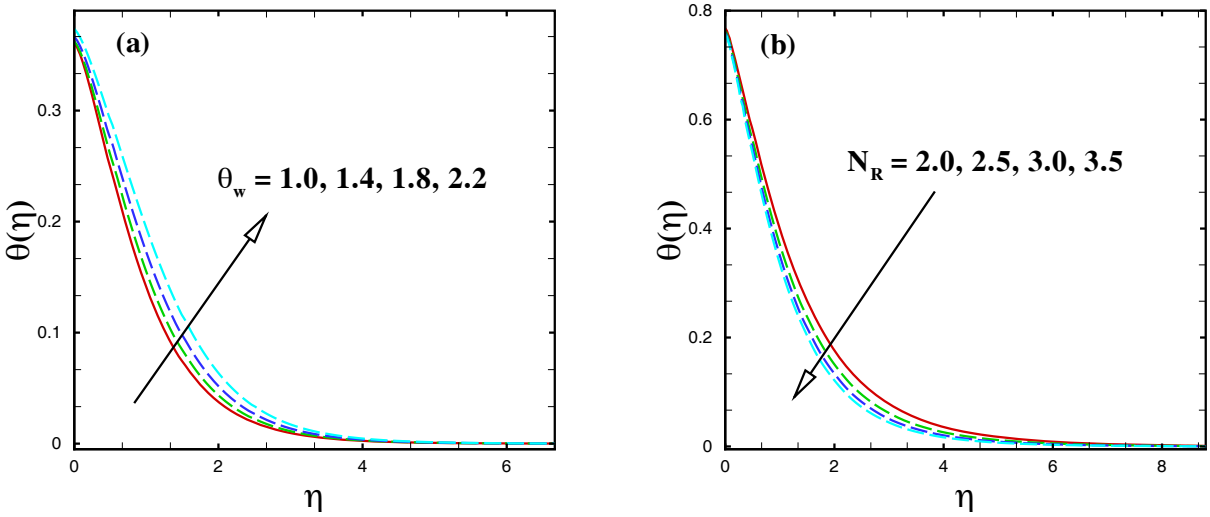

Fig. 5. The variation of θ_w and N_R on temperature profiles.

temperature parameter. Figure 5(b) shows the impact of thermal radiation on dimensionless temperature profiles. From this graph, the temperature and associated thermal boundary layer thickness depreciates for rising values of radiation parameter.

Figures 6(a) and (b) plot the similarity variable η against the impact of generalized Biot number γ on the dimensionless temperature and nanoparticle concentration. From these figures, it is noted that the temperature and nanoparticle concentration and their associated thermal and solutal boundary layer thicknesses enhance for growing values of the Biot number. The surface of the sheet is totally isolated for $\gamma = 0$. The internal thermal resistance to the surface of sheet is very strong and convective heat transfer does no take place from the surface of sheet to the cold fluid for away from the sheet. However, the recorded effect in nanoparticle volume fraction is minimal.

The behaviour of the Brownian motion parameter on the nanofluid temperature and concentration within the hydrodynamic boundary layer are shown through figs. 7(a) and (b). From these plots, it is observed that the temperature and its related thermal boundary layer thickness increase for increasing values of the Brownian motion parameter, but an opposite trend is observed for the concentration profile. The Brownian motion happens due to the presence of nanoparticles and results in the decrease in the nanoparticle volume fraction within the boundary layer region.

Figures 8(a) and (b) are drawn to show the impact of the thermophoresis parameter Nt and Schmidt number Sc on the nanoparticle concentration profiles. It is observed that the concentration field and the associated boundary solutal boundary layer thickness decreases with increasing the Nt. Since the difference between ambient and surface temperature increases for larger Nt, which increases the temperature and the concentration of the fluid. The central

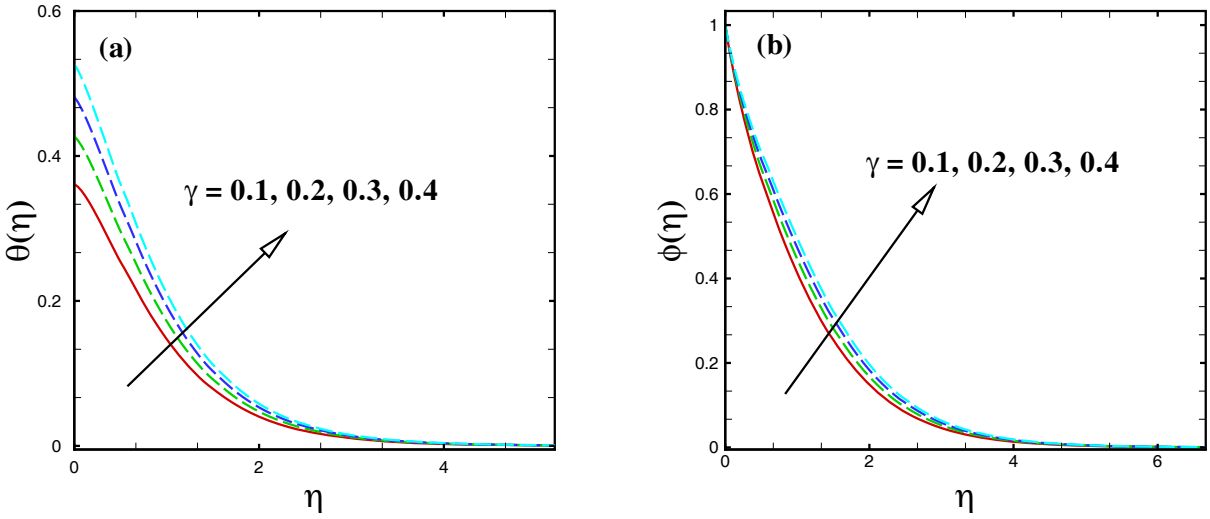

Fig. 6. The variation of γ on temperature and concentration profiles.

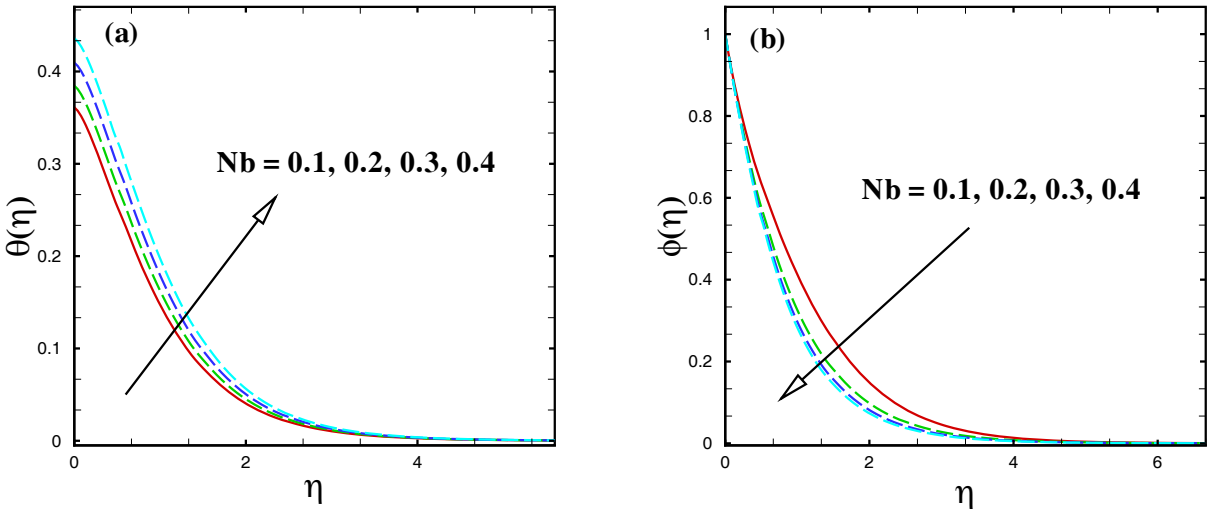

Fig. 7. The variation of Nb on temperature and concentration profiles.

reason behind this outcome is that the movement of nanoparticles from the hot area to the cold region yields an increase in the nanoparticle concentration profile. Figure 8(b) displays the effects of the Schmidt number Sc on the concentration profile. The Schmidt number embodies the ratio of kinematic viscosity to molecular mass diffusivity for an increment in Sc, which yields a reduction in mass diffusivity in the system which resulted in a decline in nanoparticle concentration.

The variation in the non-dimensional skin friction against the magnetic parameter for different values of the velocity slip parameter is shown in fig. 9(a). As was seen earlier, the fluid velocity decreases by increasing the magnetic parameter because of the Lorentz force caused by the magnetic field; consequently, the skin friction shows a similar behaviour for higher magnetic parameter, as is shown in this figure. We further noted that the dimensionless skin friction enhances as the velocity slip parameter increases. In fig. 9(b), the non-dimensional Nusselt number is sketched against the Prandtl number Pr for several values of the thermophoresis parameter Nt. These plots show that the rate of heat transfer reduces with a growth in the thermophoresis parameter. This is due to the fact that higher thermophoretic force drags the nanoparticles with large thermal conductivity from the hotter region to the ambient fluid. Further, the impact of the Prandtl number on the heat transfer rate is to enhance its magnitude. Finally, the effect of the Schmidt number on the dimensionless Sherwood number against the velocity slip parameter s_1 is depicted in fig. 9(c). This figure shows that the reduced Sherwood number increases for increasing values of the velocity slip parameter, *i.e.*, the Sherwood number is a decreasing function of s_1. It is clear from this figure that higher curves correspond to higher values of the Schmidt number Sc.

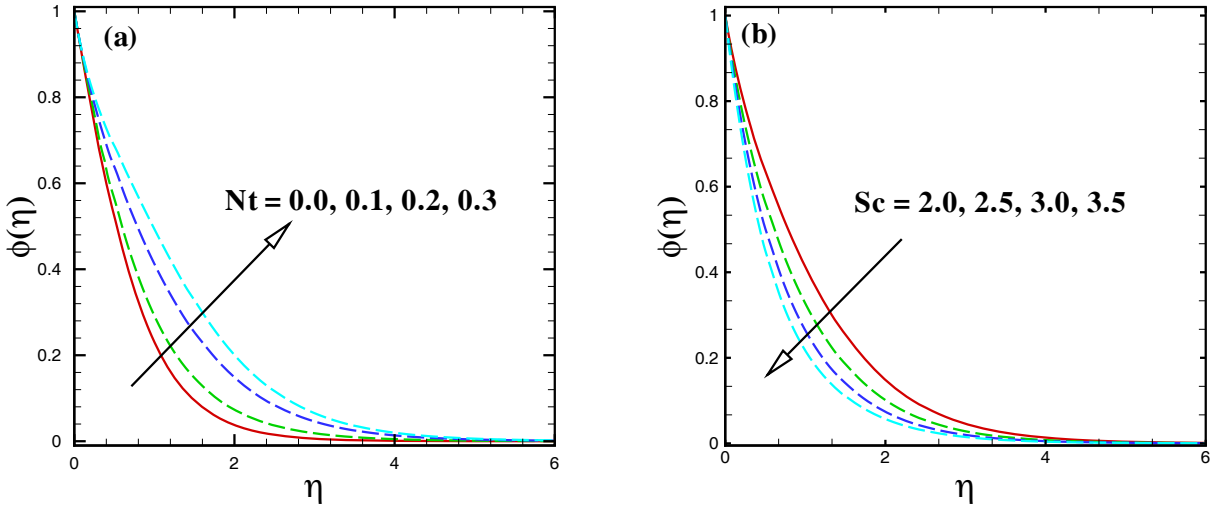

Fig. 8. The variation of Nt and Sc on concentration profiles.

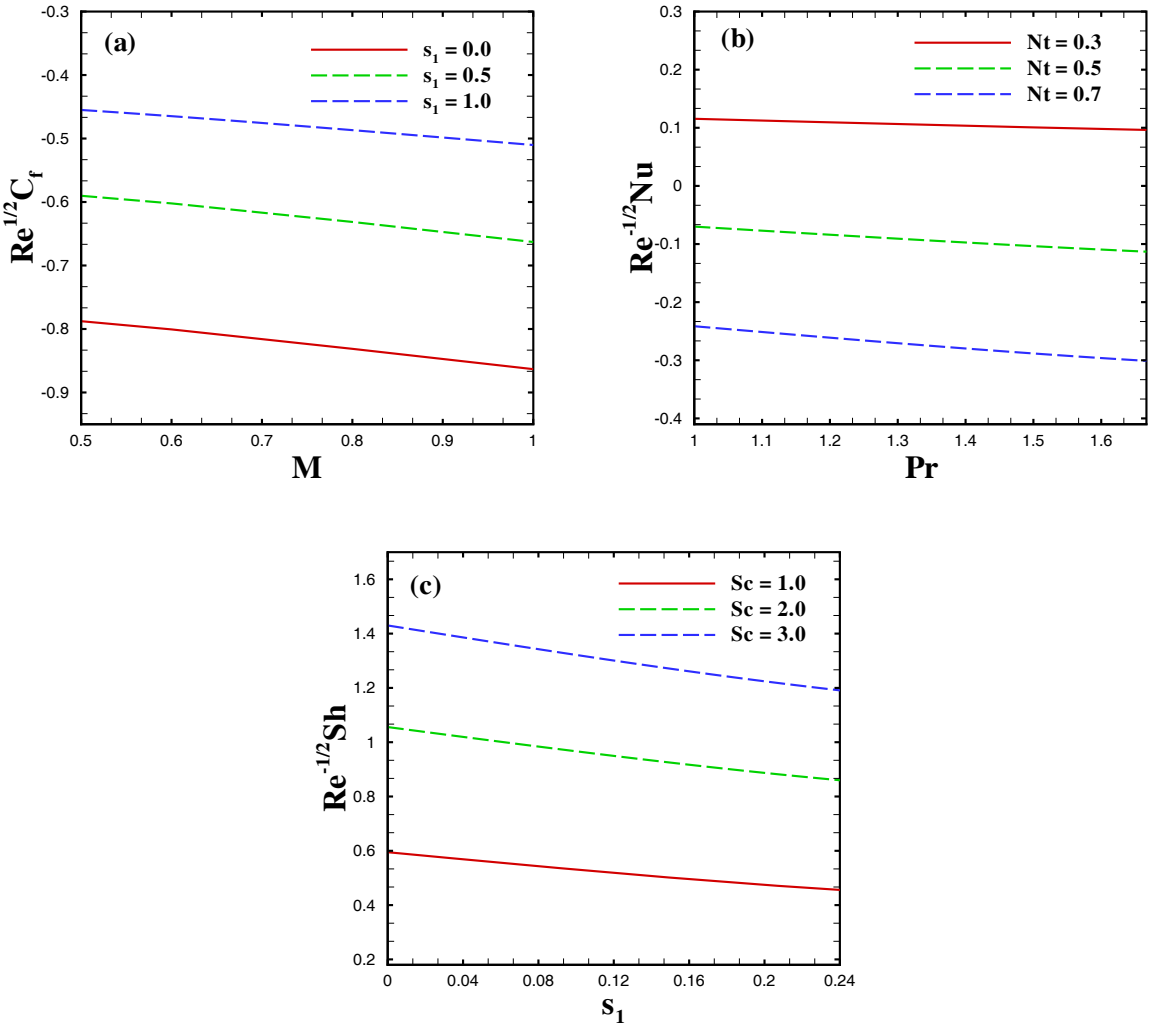

Fig. 9. The variation of s_1, Nt and Sc on $\mathrm{Re}^{1/2}\, C_{fr}$, $\mathrm{Re}^{-1/2}\, Nu_r$ and $\mathrm{Re}^{-1/2}\, Sh_r$.

5 Concluding remarks

The combined effects of transverse magnetic field, partial velocity slip, thermal radiation, thermophoresis and Brownian motion on boundary layer flow, heat and mass transfer of an electrically Williamson nanofluid were investigated numerically over a radial stretching convectively heated surface. It is concluded that:

1) The thickness of thermal and solutal boundary layers were enhanced by increase in thermophoresis forces.
2) The momentum boundary layer associated with the nanofluid velocity gets thinner with growing effects of velocity slip parameter.
3) The implementation of the magnetic force accelerated the thermal boundary layer thickness.
4) The reduced Sherwood number increases with increasing Schmidt number but decrease with increasing velocity slip parameter.

The authors gratefully acknowledge the anonymous reviewers for their valuable suggestions and comments to progress the superiority of this article.

References

1. S.U.S. Choi, *Enhancing thermal conductivity of fluids with nanoparticles*, in *Developments and Applications of Non-Newtonian Flows*, edited by D.A. Siginer, H.P. Wang, Vol. **66** (ASME, 1995) pp. 99–105.
2. J. Buongiorno, J. Heat Transf. **128**, 240 (2006).
3. D.A. Nield, A.V. Kuznetsov, Int. J. Heat Mass Transfer **52**, 5796 (2009).
4. O.D. Makinde, A. Aziz, Int. J. Therm. Sci. **53**, 2477 (2011).
5. F. Mabood, W.A. Khan, A.I.M. Ismail, J. Magn. & Magn. Mater. **374**, 569 (2015).
6. N. Sandeep, A. Malvandi, Adv. Powd. Technol. **27**, 2448 (2016).
7. Hashim, M. Khan, Int. J. Heat Mass Transfer **103**, 291 (2016).
8. S. Nadeem, A.U. Khan, S.T. Hussain, Int. J. Hydrogen Energy **42**, 28945 (2017).
9. Hashim, M. Khan, A. Hamid, Int. J. Heat Mass Transfer **118**, 480 (2018).
10. S. Mukhopadhyay, K. Bhattacharyya, G.C. Layek, Int. J. Heat Mass Transfer **54**, 2751 (2011).
11. R. Cortell, Energy **74**, 896 (2014).
12. T. Hayat, M. Imtiaz, A. Alsaedi, M.A. Kutbi, J. Magn. & Magn. Mater. **396**, 31 (2015).
13. W.A. Khan, O.D. Makinde, Z.H. Khan, Int. J. Heat Mass Transfer **96**, 525 (2016).
14. M.K. Nayak, N.S. Akbar, V.S. Pandey, Z.H. Khan, D. Tripathi, Powd. Technol. **315**, 205 (2017).
15. A.S. Dogonchi, M. Alizadeh, D.D. Ganji, Adv. Pow. Technol. **28**, 1815 (2017).
16. M. Khan, Hashim, A. Hafeez, Chem. Eng. Sci. **173**, 1 (2017).
17. J.V.R. Reddy, V. Sugunamma, N. Sandeep, J. Mol. Liq. **236**, 93 (2017).
18. N. Sandeep, M.G. Reddy, J. Mol. Liq. **225**, 87 (2017).
19. R.V. Williamson, Ind. Eng. Chem. **21**, 1108 (1929).
20. I. Dapra, G. Scarpi, Int. J. Rock Mech. Min. Sci. **44**, 271 (2007).
21. C. Vasudev, U.R. Rao, M.V.S. Reddy, G.P. Rao, Am. J. Sci. Ind. Res. **1**, 656 (2010).
22. S. Nadeem, S.T. Hussain, C. Lee, Braz. J. Chem. Eng. **30**, 619 (2013).
23. S. Nadeem, N.S. Akbar, Int. J. Numer. Methods Fluids **66**, 212 (2010).
24. M.M. Bhatti, M.M. Rashidi, J. Mol. Liq. **221**, 567 (2016).
25. S. Reddy, K. Naikoti, M.M. Rashidi, Trans. A. Razmadze Math. Inst. **171**, 195 (2017).
26. G. Kumaran, N. Sandeep, J. Mol. Liq. **233**, 262 (2017).
27. S. Rosseland, *Astrophysik und Atom-Theoretische Grundlagen* (Springer Verlag, Berlin, 1931) pp. 41–44.
28. P.D. Ariel, Int. J. Comput. Math. Appl. **54**, 69 (2007).
29. O.D. Makinde, F. Mabood, W.A. Khan, M.S. Tshehla, J. Mol. Liq. **219**, 24 (2016).